AIMS Mathematics, 11(4): 11347–11371.
DOI: 10.3934/math.2026467
Received: 02 January 2026
Revised: 23 March 2026
Accepted: 08 April 2026
Published: 22 April 2026

https://www.aimspress.com/journal/Math

Research article

An extended $\frac{G'}{G}$-expansion method for the conformable space-time fractional Newell-Whitehead-Segel equation: Exact traveling-wave solutions and regularity features

Chunyan Zhao[1,*], **Jie Wu**[2] **and Zheng Yang**[3]

[1] Department of Mathematics, Sichuan University Jinjiang College, Meishan 620860, China
[2] College of Computer Science, Chengdu University, Chengdu 610106, China
[3] Sichuan University-Pittsburgh Institute, Chengdu 610299, China

* **Correspondence:** Email: zhaochunyan_007@163.com.

Abstract: This paper employed an extended $\frac{G'}{G}$-expansion method to investigate the conformal fractional Newell-Whitehead-Segel equation. By applying a traveling-wave transformation, we derive three types of analytical solutions that describe this fractional equation, thereby providing a useful theoretical foundation and intuitive interpretation for understanding its dynamical behavior. Analysis of the obtained solutions revealed that when both spatiotemporal orders approach 1, the regularity of the solutions becomes highly complex in a specific region. However, when one of the parameters λ or μ is taken as 1 and the other as 0, the regularity region is significantly improved. Furthermore, the comparison showed that the regularity becomes worse as $\frac{\lambda+\mu}{2}$ increases. The corresponding contour plots serve as a clear supplement to the complex variations in regularity. We also considered the influence of the parameter k on the solutions: larger values of k lead to more singularities in the solutions and increase the likelihood of blow-up, while smaller values of k reduce singularities and promote the global existence of the solutions.

Keywords: conformable fractional Newell-Whitehead-Segel; $\frac{G'}{G}$-expansion method; exact solutions
Mathematics Subject Classification: 35C07, 35G25, 35G60, 35K10, 35K55, 35R11

1. Introduction

In science and engineering, partial differential equations (PDEs) are ubiquitous and play a crucial role in modeling and analyzing many complex phenomena. Typical examples include elliptic and parabolic equations from mathematics, hyperbolic equations describing string vibrations, and the Navier-Stokes equations governing fluid motion. Over the past decades, the study of these equations

has developed into a rich theoretical framework. Researchers have employed tools such as a priori estimates, variational methods, continuity methods, and the moving-plane method to systematically investigate fundamental issues including existence and uniqueness of solutions, asymptotic behavior, multiplicity of solutions, regularity, and maximum principles. These advances provide a solid theoretical foundation for further research on integer-order PDEs.

However, space-time fractional partial differential equations offer distinctive advantages for modeling real-world dynamical processes. Therefore, it is important to develop theories and analytical methods tailored to fractional-order equations. One representative example is the Newell-Whitehead-Segel equation (NWSE) [10, 18, 27, 32, 38], an important class of reaction-diffusion equations that originated in the study of Turing pattern formation. It describes the dynamical process in systems far from equilibrium, such as heated fluids or chemical reaction systems, where diffusion driven instability interacts with nonlinear reactions, leading to the spontaneous emergence of stable spatial stripe patterns from a homogeneous state. The equation can be written as

$$k\frac{\partial u(x,t)}{\partial t} - a\frac{\partial^2 u(x,t)}{\partial x^2} + bu^p(x,t) - u(x,t) = 0, \tag{1.1}$$

where k, a, and b are constants. Specifically, the parameter k typically represents the system's response rate to temporal changes or the damping of the magnitude. If viewed in the context of generalized heat or diffusion equations, k is sometimes analogous to heat capacity or a time constant. A large k indicates greater temporal inertia of the system, meaning its state changes more sluggishly over time; a smaller k implies a faster response to changes. As $k \to 0$, the system's time dependence vanishes, and it instantaneously reaches a steady state. Physically, this corresponds to an approximation that neglects the temporal inertia term. Parameter a is the diffusion coefficient. It determines the smoothing capability or propagation speed of the physical quantity in space. If $a > 0$, the equation is parabolic, exhibiting a smoothing effect where local Gaussian disturbances broaden over time. In pattern formation dynamics, the magnitude of a dictates the range of interaction. A large a leads to smoother, larger-scale spatial structures, while a smaller a allows for the emergence of sharp gradients (such as spikes). Parameter b is the nonlinear coefficient, which usually represents the strength of the nonlinear source term. When $b > 0$, it denotes a growth term or activation term; when $b < 0$, it represents a consumption term or inhibition term. Here, $u(x,t)$ represents the distribution function (or concentration) of particles along the spatial coordinate x in a liquid or solid medium. The term $\frac{\partial u}{\partial t}$ describes the temporal variation of u, while the diffusion term $\frac{\partial^2 u}{\partial x^2}$ captures spatial spreading and smoothing. The linear term u represents a linear growth, whereas $-bu^p$ accounts for nonlinear reaction effects. In particular, the nonlinear term acts as a saturation mechanism that prevents unbounded growth of solutions and plays a crucial role in pattern stabilization. Equation (1.1) is also referred to as the NWSE. Local existence of solutions can be established via the Banach fixed-point theorem; see [20, 48, 49, 51] for details. With suitable a priori estimates, one can further obtain global solutions. As $k \to 0$, the equation degenerates into an elliptic equation. For studies of the limiting process from the parabolic case to the elliptic one, see [17, 46]. Moreover, if $|a|$ is sufficiently large and $ab < 0$, the mountain pass theorem [6, 22] can be used to obtain nontrivial solutions $u(x) \neq 0$ of (1.1). Here, we provide a simplified proof.

In fact, we assume that (1.1) takes the following form:

$$-\frac{\partial^2 u(x)}{\partial x^2} = mu^p(x) + nu(x), \tag{1.2}$$

where $m = -\frac{b}{a} > 0$, $n = \frac{1}{a} \ll 1$. Suppose that $x \in [a_1, a_2] := I$, where $a_1, a_2 \in \mathbb{R}$ and I is an interval.

Let $E = W_0^{1,2}(I)$ and define the function

$$J(u) = \frac{1}{2}\int_{a_1}^{a_2} \left|\frac{\partial u}{\partial x}\right|^2 dx - \frac{m}{p+1}\int_{a_1}^{a_2} u^{p+1} dx - \frac{n}{2}\int_{a_1}^{a_2} u^2 dx. \tag{1.3}$$

Obviously, $J(0) = 0$. Applying Young's inequality in (1.3), we can obtain

$$\begin{aligned} J(u) &\geq \frac{1}{2}\|u\|_E^2 - \frac{m}{p+1}\|u\|_{p+1}^{p+1} - \frac{C_1 n}{2}\|u\|_E^2 \\ &\geq \frac{1 - C_1 n}{2}\|u\|_E^2 - \frac{m}{p+1}\|u\|_{p+1}^{p+1} \\ &\geq \frac{1 - C_1 n}{2}\|u\|_E^2 \left(1 - \frac{2m}{(p+1)(1-C_1 n)}\|u\|_E^{p-1}\right). \end{aligned}$$

Since $|a|$ is large enough, it can ensure that $\frac{1-C_1 n}{2} > 0$. Taking $\rho = \left[\frac{(p+1)(1-C_1 n)}{4m}\right]^{\frac{1}{p-1}}$, we have

$$J(u) \geq \frac{1 - C_1 n}{4}\rho^2 := \alpha > 0 \quad \text{as } \|u\|_E = \rho.$$

Thus, we get $J\big|_{\partial B_\rho(0)} = \alpha > 0$.

On the other hand, we can obtain

$$J(tu) \geq \frac{t^2}{2}\int_{a_1}^{a_2} \left|\frac{\partial u}{\partial x}\right|^2 dx - \frac{mt^{p+1}}{p+1}\int_{a_1}^{a_2} |u|^{p+1} dx - \frac{nt^2}{2}\int_{a_1}^{a_2} |u|^2 dx \to -\infty \quad \text{as } t \to +\infty.$$

Thus, there exists $t > \rho$ such that

$$J(tu) \leq 0.$$

This proves that there is an $e = tu \in E\backslash\overline{B_\rho(0)}$ satisfying $I(e) \leq 0$.

In the end, we prove that J satisfies the Palais-Smale condition. Suppose that $\{u_m\} \subset W_0^{1,2}(I)$ satisfies

$$\begin{aligned} &|J(u_m)| \leq M, \quad m = 1, 2, \cdots, \\ &J'(u_m) \to 0, \quad \text{in } (W_0^{1,2}(I))^* \quad \text{as } m \to \infty. \end{aligned} \tag{1.4}$$

Next, we only need to show that $\{u_m\}$ is bounded in $W_0^{1,2}(I)$. Using the second condition of (1.4), there is $m_0 \in \mathbb{N}$ such that

$$\|J'(u_m)\| \leq 1 \quad \text{as } m \geq m_0.$$

Therefore, we have

$$|\langle J'(u_m), \phi\rangle| \leq \|\phi\|_{W_0^{1,2}(I)} \quad \forall \phi \in W_0^{1,2}(I),\ m \geq m_0.$$

Thus, we can apply (1.4) to obtain

$$\begin{aligned}\Big(\frac{p}{2}-1\Big)\|u_m\|_E^2 &= pJ(u_m) - \langle J'(u_m), u_m\rangle - \frac{n(p-1)}{2}\int_{a_1}^{a_2} u_m^2 dx \\ &\le p|J(u_m)| + \|u_m\|_E + \int_{a_1}^{a_2} \max_{x\in I,\,|u_m|\le r} u_m^2 dx \\ &\le pM + \|u_m\|_E + C_2 \quad \text{as} \ \ m \ge m_0.\end{aligned}$$

Using the Young's inequality for the above equation, we can obtain

$$\|u_m\| \le C_3,$$

where C_2, C_3 are positive constants. Therefore, using the mountain path theorem, it is known that the functional has a critical value c and there exists a critical point $u \in E$ such that $J'(u) = 0$. That is,

$$\langle J'(u), \phi\rangle = \int_{a_1}^{a_2} [u_x\phi_x - \int_{a_1}^{a_2} (mu^p + nu)dx = 0.$$

Thus, Eq (1.2) has a weak solution $u \in W_0^{1,2}(I)$ and $J(u) = c \ge \alpha > 0$. We get $u \ne 0$, hence, u is a nontrivial solution.

With the introduction of the conformable fractional derivative defined in Section 2, the classical derivative is recovered as the special case where $\lambda = \mu = 1$. Consequently, this derivative exhibits richer properties that merit further investigation. As a result, researchers moved beyond integer-order models and widely adopted fractional derivatives to reformulate the NWSE. The conformable space-time fractional version of the model can be expressed as follows:

$$kD_t^{\mu}u(x,t) - aD_{xx}^{\lambda}u(x,t) + bu^p(x,t) - u(x,t) = 0, \tag{1.5}$$

where $k, a, b > 0,\ p = 3$, and the parameters $\lambda,\ \mu \in (0, 1]$.

The introduction of the conformable fractional derivative renders most of the analytical techniques and tools from the classical Sobolev space framework inapplicable. This necessitates the development of specialized methods and techniques, leading to a wealth of outstanding research achievements. For instance, methods for handling common fractional derivatives can be found in [2–4, 8, 14, 15, 23, 26, 30, 33, 35, 40, 41, 43, 44, 52, 56], studies on the Riemann-Liouville derivative are available in [9, 24, 28, 34, 37], and works on the Caputo derivative are referenced in [1, 5, 11, 36, 39]. Here, we introduce a $\frac{G'}{G}$-expansion method particularly suited for solving such problem in [21, 53], which has become a widely used approach for deriving exact solutions of fractional-order equations of the form above. Numerous related works have appeared; see [7, 12, 13, 16, 29, 31, 42, 45, 50, 54, 55, 57–59]. Recently, the analytical properties, bifurcation, sensitivity, and chaotic behavior of the fractional Klein-Gordon equation were investigated in [19].

The remainder of this paper is organized as follows. In Section 2, we present the definition of the conformable fractional derivative and the analytical solution process for the NWSE. Based on the exact solutions obtained, numerical simulations and analyses are carried out in Section 3. Finally, a qualitative description of the solutions is provided through the corresponding graphical illustrations.

2. Method of the conformable fractional Newell-Whitehead-Segel equation

2.1. Conformable fractional derivatives

We begin by recalling the definition of conformable fractional derivatives $D_{t,x}^{\mu,\lambda}$ from [25, 50]. They can be viewed as a special type of variation, defined as follows:

Definition 2.1. *For a function $f : (0, +\infty) \to \mathbb{R}$, the conformable fractional derivative of order μ is defined by*

$$D_t^{\mu} f(t) = \lim_{\epsilon \to 0} \frac{f(t + \epsilon t^{1-\mu}) - f(t)}{\epsilon}.$$

By virtue of Definition 2.1, an operator D_x^{λ} with completely analogous properties can be introduced. From this definition, a remark follows naturally.

Remark 2.1. *(Derivative rules) For any $\mu \in (0, 1]$, we have*
(1) $D_t^{\mu}(af(t) + bg(t)) = aD_t^{\mu} f(t) + bD_t^{\mu} g(t)$;
(2) $D_t^{\mu}(t^q) = qt^{q-\mu}$ for all $q \in \mathbb{R}$;
(3) $D_t^{\mu}\big(f(t)g(t)\big) = f(t)D_t^{\mu} g(t) + g(t)D_t^{\mu} f(t)$;
(4) $D_t^{\mu}\Big(\frac{f(t)}{g(t)}\Big) = \frac{g(t)D_t^{\mu} f(t) - f(t)D_t^{\mu} g(t)}{g^2(t)}$.

In this section, we apply the extended-$\left(\frac{G'}{G}\right)$-expansion method [21] to find the exact solutions of (1.5). In order to obtain the exact solution of Eq (1.5), we need to perform the following traveling wave transformation:

$$u(x, t) = u(\xi), \tag{2.1}$$

where $\xi = \frac{x^{\lambda}}{\lambda} - c\frac{t^{\mu}}{\mu}$. Thus, using the chain rule for (2.1), we can get

$$D_t^{\mu} u(x, t) = u'(\xi) D_t^{\mu}\left(\frac{x^{\lambda}}{\lambda} - c\frac{t^{\mu}}{\mu}\right) = -cu'(\xi) \tag{2.2}$$

and

$$D_{xx}^{\lambda} u(x, t) = D_x^{\lambda}\left[u'(\xi) D_x^{\lambda}\left(\frac{x^{\lambda}}{\lambda} - c\frac{t^{\mu}}{\mu}\right)\right] = u''(\xi). \tag{2.3}$$

Substituting Eqs (2.2) and (2.3) into (1.5), we have

$$u''(\xi) + \frac{kc}{a}u'(\xi) - \frac{b}{a}u^3(\xi) + \frac{1}{a}u(\xi) = 0. \tag{2.4}$$

We can use the extended-$\frac{G'}{G}$-expansion method to obtain the exact solutions. Let

$$u(\xi) = \sum_{i=-m}^{m} d_i \left(\frac{G'}{G}\right)^i, \tag{2.5}$$

where G satisfies the following ordinary differential equation:

$$\frac{G''}{G} = \alpha\left(\frac{G'}{G}\right)^2 + \beta\left(\frac{G'}{G}\right) + \gamma. \tag{2.6}$$

Let $\Delta = \beta^2 - 4\alpha(\alpha-1)\gamma \ \ (\alpha \neq 1)$. We use the methods of [50] to obtain

$$\frac{G'(\xi)}{G(\xi)} = \begin{cases} \frac{\sqrt{\Delta}}{2(1-\alpha)}\left(\frac{C_1\sinh(\frac{\sqrt{\Delta}}{2}\xi)+C_2\cosh\frac{\sqrt{\Delta}}{2}\xi}{C_1\cosh(\frac{\sqrt{\Delta}}{2}\xi)+C_2\sinh\frac{\sqrt{\Delta}}{2}\xi}\right)+\frac{\beta}{2(1-\alpha)}, & \Delta>0,\ \alpha\neq 1; \\ \frac{\sqrt{-\Delta}}{2(1-\alpha)}\left(\frac{-C_1\sin(\frac{\sqrt{-\Delta}}{2}\xi)+C_2\cos(\frac{\sqrt{-\Delta}}{2}\xi)}{C_1\cos(\frac{\sqrt{-\Delta}}{2}\xi)+C_2\sin(\frac{\sqrt{-\Delta}}{2}\xi)}+\frac{\beta}{2(1-\alpha)}\right), & \Delta<0,\ \alpha\neq 1; \\ \frac{1}{1-\alpha}\left(\frac{C_1}{C_1\xi+C_2}+\frac{\beta}{2}\right), & \Delta=0,\ \alpha\neq 1. \end{cases} \tag{2.7}$$

To obtain the exact solutions of (2.4), we need to utilize the principle of the homogeneous balance method in [47] to determine the index of m. Here,

$$\deg(u'') = \deg(u^3). \tag{2.8}$$

Thus, we can obtain

$$m+2 = 3m, \quad (\alpha-1)^2 m(m+1) = d_m^2, \quad m(m+1)\gamma^2 = \frac{b}{a}d_{-m}^2. \tag{2.9}$$

So, by solving (2.9), we have

$$m = 1, \quad d_1 = \pm\sqrt{\frac{2a}{b}}(\alpha-1), \quad d_{-1} = \pm\sqrt{\frac{2a}{b}}\gamma. \tag{2.10}$$

Substituting (2.10) into (2.5), we obtain

$$u(\xi) = d_0 + d_1\frac{G'}{G} + d_{-1}\left(\frac{G'}{G}\right)^{-1}. \tag{2.11}$$

Therefore, plugging (2.11) into (2.4) and comparing the coefficients of $\left(\frac{G'}{G}\right)^2$ and $\left(\frac{G'}{G}\right)^{-2}$, we get

$$\frac{kc}{a}d_1(\alpha-1) - \frac{3b}{a}d_0d_1^2 + 3d_1(\alpha-1)\beta = 0 \tag{2.12}$$

and

$$-\frac{kc}{a}d_{-1}\gamma - 3d_0d_{-1}^2\frac{b}{a} + 3d_{-1}\beta\gamma = 0. \tag{2.13}$$

Solving (2.12) and (2.13), we can get

$$c = \frac{3}{k}\left(\frac{bd_0d_1}{\alpha-1} - a\beta\right) = \frac{3}{k}(a\beta - \frac{bd_0d_{-1}}{\gamma}). \tag{2.14}$$

Similarly, comparing the coefficients of $\left(\frac{G'}{G}\right)$ and $\left(\frac{G'}{G}\right)^{-1}$, we can obtain

$$-\frac{kc\beta}{a} - \frac{3b}{a}(d_0^2 + d_1d_{-1}) + \frac{1}{a} + \beta^2 + 2(\alpha-1)\gamma = 0 \tag{2.15}$$

and

$$\frac{kc\beta}{a} - \frac{3b}{a}(d_0^2 + d_1d_{-1}) + \frac{1}{a} + \beta^2 + 2(\alpha-1)\gamma = 0. \tag{2.16}$$

Applying (2.15) and (2.16), we deduce that

$$\beta = 0, \quad 3b(d_0^2 + d_1 d_{-1}) = 1 + 2a(\alpha - 1)\gamma. \tag{2.17}$$

By comparing the constant terms, one has

$$d_1\beta\gamma + d_{-1}(\alpha - 1)\beta + \frac{kc}{a}[d_1\gamma - d_{-1}(\alpha - 1)] - \frac{b}{a}(d_0^3 + 6d_0 d_1 d_{-1}) + \frac{d_0}{a} = 0. \tag{2.18}$$

Applying (2.14) and (2.17), we can deduce that

$$d_1\gamma = d_{-1}(1 - \alpha), \quad c = \frac{3bd_0 d_1}{k(\alpha - 1)}. \tag{2.19}$$

Thanks to (2.17)–(2.19), we have

$$b(d_0^2 + 12d_1 d_{-1}) = 1. \tag{2.20}$$

By comparing (2.10) and (2.19), we can deduce that

$$\gamma = 0,\ d_{-1} = 0 \quad \text{or} \quad \gamma \neq 0,\ d_1 \mathrm{d}_{-1} < 0. \tag{2.21}$$

However, if $\gamma = \beta = d_{-1} = 0$, we can derive contradiction through (2.15) and (2.18). Therefore, $\beta = 0$ and $\gamma = 0$ cannot both hold simultaneously. Using (2.20) and (2.21), we can obtain

$$d_0 = \pm\sqrt{\frac{1 - 24a(1 - \alpha)\gamma}{b}}. \tag{2.22}$$

Using (2.17), (2.20), and (2.21), we have

$$a(1 - \alpha)\gamma = \frac{1}{32}. \tag{2.23}$$

By virtue of (2.22) and (2.23), we can get

$$d_0 = \pm\frac{1}{2\sqrt{b}}. \tag{2.24}$$

Applying (2.10), (2.19), and (2.24), we can obtain the values of d_1, d_{-1}, d_0, and c in the following Table 1.

Table 1. The coefficients of the $\frac{G'}{G}$-expansion.

d_1	d_{-1}	d_0	c
$\sqrt{\frac{2a}{b}}(\alpha - 1)$	$-\sqrt{\frac{2a}{b}}\gamma$	$\frac{1}{2\sqrt{b}}$	$\frac{3\sqrt{2a}}{2k}$
$\sqrt{\frac{2a}{b}}(\alpha - 1)$	$-\sqrt{\frac{2a}{b}}\gamma$	$-\frac{1}{2\sqrt{b}}$	$-\frac{3\sqrt{2a}}{2k}$
$-\sqrt{\frac{2a}{b}}(\alpha - 1)$	$\sqrt{\frac{2a}{b}}\gamma$	$\frac{1}{2\sqrt{b}}$	$-\frac{3\sqrt{2a}}{2k}$
$-\sqrt{\frac{2a}{b}}(\alpha - 1)$	$\sqrt{\frac{2a}{b}}\gamma$	$-\frac{1}{2\sqrt{b}}$	$\frac{3\sqrt{2a}}{2k}$

Through traveling wave transformation, we obtain three types of exact solutions: hyperbolic, rational, and trigonometric function solutions. These solutions provide complementary insights into the pattern formation and nonlinear dynamics described by the conformal fractional NWSE.

Hyperbolic function solutions correspond to kink or shock wave structures, characterizing transition interfaces between distinct stable states. In the context of the NWSE, these solutions typically represent phase boundaries or traveling wave fronts during pattern formation, reflecting the nonlinear transition from one uniform state to another. The inclusion of fractional derivatives introduces power-law dependence in both the thickness and propagation speed of the transition region, highlighting the nonlocal memory effects inherent to the system.

Rational function solutions often exhibit algebraic decay or isolated singularities and are capable of describing rogue waves or transient burst events. In pattern-forming systems, such solutions correspond to localized high-amplitude structures that may emerge near critical points or bifurcation boundaries. Their appearance generally indicates heightened sensitivity to initial conditions or parameter perturbations, underscoring the role of long-range correlations in the stability of fractional-order patterns.

Trigonometric function solutions correspond to periodic or standing wave structures, describing regular patterns such as stripes and hexagons. In the NWSE, these solutions serve as fundamental modes in linear stability analysis and also arise as approximate solutions of the Ginzburg-Landau equation in weakly nonlinear regimes. Varying the fractional-order parameters alters the dispersion relations and modulation instability conditions, thereby influencing pattern selection.

In summary, hyperbolic solutions capture the propagation and competition of pattern boundaries, rational solutions reveal localized structures and critical fluctuations, and trigonometric solutions describe fundamental periodic modes. The introduction of fractional-order parameters enables richer control over the regularity, stability, and propagation behavior of these solutions compared to their integer-order counterparts, offering new mathematical tools and physical insights for theoretical studies of pattern dynamics, experimental design, and engineering applications such as micro-fluidics and materials patterning.

Next, we will provide the special values of d_0, d_1, d_{-1}, and c for different cases about $a, b, k > 0$ and $\alpha, \gamma \in \mathbb{R}$ in Tables 2–6.

Table 2. Parameter values for different discriminant cases.

Case	α	β	γ	Δ	$\frac{G'}{G}$ $(\xi = \frac{x^\lambda}{\lambda} - c\frac{t^\mu}{\mu})$
$\Delta > 0$	2	0	$-\frac{1}{32}$	$\frac{1}{4}$	$-\frac{\tanh\frac{\xi}{4} + C}{4\left(1 + C\tanh\frac{\xi}{4}\right)}$
$\Delta = 0$	0	0	$\frac{1}{32}$	0	$\frac{1}{\xi + C}$
$\Delta < 0$	-1	0	$\frac{1}{64}$	$-\frac{1}{8}$	$\frac{1}{8\sqrt{2}} \cdot \frac{-\tan\frac{\xi}{4\sqrt{2}} + C}{1 + C\tan\frac{\xi}{4\sqrt{2}}}$

Table 3. Coefficient values for different cases ($a = 2, b = 1, k = 1$).

Case 1	Row	d_1	d_{-1}	d_0	$c_{k=1}$
$\Delta > 0$	1	2	$\frac{1}{16}$	$\frac{1}{2}$	3
	2	2	$\frac{1}{16}$	$-\frac{1}{2}$	-3
	3	-2	$-\frac{1}{16}$	$\frac{1}{2}$	-3
	4	-2	$-\frac{1}{16}$	$-\frac{1}{2}$	3
$\Delta = 0$	1	-2	$-\frac{1}{16}$	$\frac{1}{2}$	3
	2	-2	$-\frac{1}{16}$	$-\frac{1}{2}$	-3
	3	2	$\frac{1}{16}$	$\frac{1}{2}$	-3
	4	2	$\frac{1}{16}$	$-\frac{1}{2}$	3
$\Delta < 0$	1	-4	$-\frac{1}{32}$	$\frac{1}{2}$	3
	2	-4	$-\frac{1}{32}$	$-\frac{1}{2}$	-3
	3	4	$\frac{1}{32}$	$\frac{1}{2}$	-3
	4	4	$\frac{1}{32}$	$-\frac{1}{2}$	3

Table 4. Coefficient values for $k = 0.001$ with fixed $a = 2, b = 1$.

Case 2	Row	d_1	d_{-1}	d_0	$c_{k=0.001}$
$\Delta > 0$	1	2	$\frac{1}{16}$	$\frac{1}{2}$	3000
	2	2	$\frac{1}{16}$	$-\frac{1}{2}$	-3000
	3	-2	$-\frac{1}{16}$	$\frac{1}{2}$	-3000
	4	-2	$-\frac{1}{16}$	$-\frac{1}{2}$	3000
$\Delta = 0$	1	-2	$-\frac{1}{16}$	$\frac{1}{2}$	3000
	2	-2	$-\frac{1}{16}$	$-\frac{1}{2}$	-3000
	3	2	$\frac{1}{16}$	$\frac{1}{2}$	-3000
	4	2	$\frac{1}{16}$	$-\frac{1}{2}$	3000
$\Delta < 0$	1	-4	$-\frac{1}{32}$	$\frac{1}{2}$	3000
	2	-4	$-\frac{1}{32}$	$-\frac{1}{2}$	-3000
	3	4	$\frac{1}{32}$	$\frac{1}{2}$	-3000
	4	4	$\frac{1}{32}$	$-\frac{1}{2}$	3000

Table 5. Coefficient values for two different cases d_0, d_1, and d_{-1}.

Case 3	Row	d_1	d_{-1}	d_0	c
$\Delta > 0$	1	2	$\frac{1}{16}$	$\frac{1}{2}$	3
	2	2	$\frac{1}{16}$	$-\frac{1}{2}$	-3
$\Delta = 0$	1	-2	$-\frac{1}{16}$	$\frac{1}{2}$	3
	2	-2	$-\frac{1}{16}$	$-\frac{1}{2}$	-3
$\Delta < 0$	1	-4	$-\frac{1}{32}$	$\frac{1}{2}$	3
	2	-4	$-\frac{1}{32}$	$-\frac{1}{2}$	-3

Table 6. Parameter combinations for λ and μ.

Case	λ	μ
$a = 2, b = 1, k = 1$	0.1	0.1
	0.4	0.4
	0.7	0.7
	1.0	1.0
$a = 2, b = 1, k = 1$	0.1	1.0
	0.4	0.7
	0.7	0.4
	1.0	0.1

Case 1: The first set of data shows the situation when $a = 2, b = 1, k = 1$, and $\lambda = \mu = 0.5$ are fixed and different values α and γ are taken.
If $\lambda = \mu = 0.5$ and $C = 2$, then we have

$$\Delta > 0, \qquad \frac{G'}{G} = \begin{cases} -\frac{2+\tanh\frac{\sqrt{x}-3\sqrt{t}}{2}}{4\left(1+2\tanh\frac{\sqrt{x}-3\sqrt{t}}{2}\right)}, & c = 3, \\ -\frac{2+\tanh\frac{\sqrt{x}+3\sqrt{t}}{2}}{4\left(1+2\tanh\frac{\sqrt{x}+3\sqrt{t}}{2}\right)}, & c = -3, \end{cases}$$

$$\Delta = 0, \qquad \frac{G'}{G} = \begin{cases} \frac{1}{2+2\sqrt{x}-6\sqrt{t}}, & c = 3, \\ \frac{1}{2+2\sqrt{x}+6\sqrt{t}}, & c = -3, \end{cases}$$

$$\Delta < 0, \qquad \frac{G'}{G} = \begin{cases} \frac{1}{8\sqrt{2}} \cdot \frac{-\tan\frac{\sqrt{x}-3\sqrt{t}}{2\sqrt{2}}+2}{1+2\tan\frac{\sqrt{x}-3\sqrt{t}}{2\sqrt{2}}}, & c = 3, \\ \frac{1}{8\sqrt{2}} \cdot \frac{-\tan\frac{\sqrt{x}+3\sqrt{t}}{2\sqrt{2}}+2}{1+2\tan\frac{\sqrt{x}+3\sqrt{t}}{2\sqrt{2}}}, & c = -3. \end{cases}$$

Case 2: In the second set of data, we fixed $a = 2, b = 1$, and $\lambda = \mu = 0.5$, and obtained different parameter scenarios for $k = 0.001$.
Case 3: In the third set of data, we fixed the values of $a = 2, b = 1$, and $k = 1$, took different values of λ and μ in Table 3, and obtained the following Table 5. For simplicity, we selected two scenarios for each of $\Delta > 0$, $\Delta = 0$, and $\Delta < 0$ in Table 5.
Table 6 presents two sets of λ and μ values with a, b, and k fixed. In the first set, λ and μ are equal and increase from 0.1 to 1 by a step of 0.3. In the second set, they follow opposite trends: λ increases monotonically while μ decreases monotonically.

3. Image discussion

The subfigures (a)–(d) of Figures 1–3 correspond to the different parameter settings listed in Table 3. The associated contour plots of Figure 4–6 were generated in Maple using the contourplot function. These contour plots are horizontal slices (projections) of the corresponding three-dimensional surface

plots, analogous to contour lines on a topographic map. Regions with densely packed contours indicate rapid variation in the function (large gradients), whereas more widely spaced contours indicate slower changes. In general, blue (cool colors) represents smaller values and red (warm colors) represents larger values.

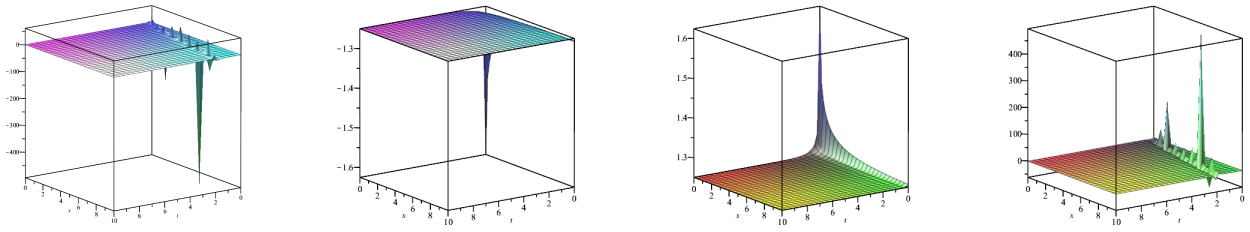

(a) $c = 3$ **(b)** $c = -3$ **(c)** $c = -3$ **(d)** $c = 3$

Figure 1. $\Delta > 0, C_2 = 2C_1, \lambda = \mu = 0.5$ in Tables 2 and 3.

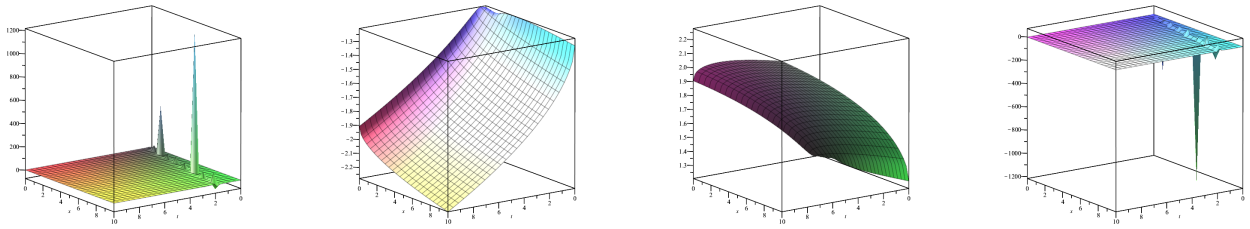

(a) $c = 3$ **(b)** $c = -3$ **(c)** $c = -3$ **(d)** $c = 3$

Figure 2. $\Delta = 0, C_2 = 2C_1, \lambda = \mu = 0.5$ in Tables 2 and 3.

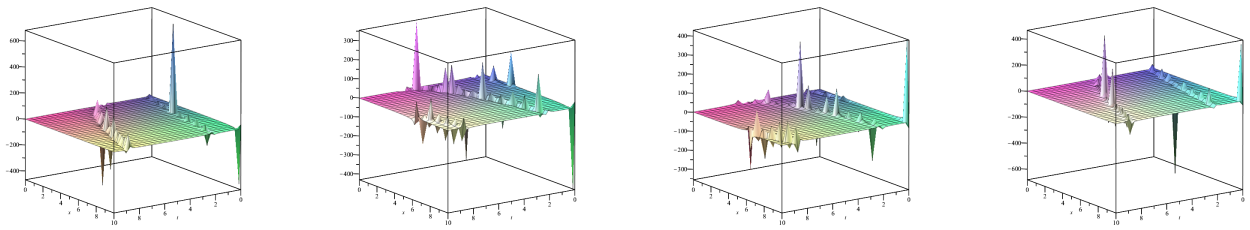

(a) $c = 3$ **(b)** $c = -3$ **(c)** $c = -3$ **(d)** $c = 3$

Figure 3. $\Delta < 0, C_2 = 2C_1, \lambda = \mu = 0.5$ in Tables 2 and 3.

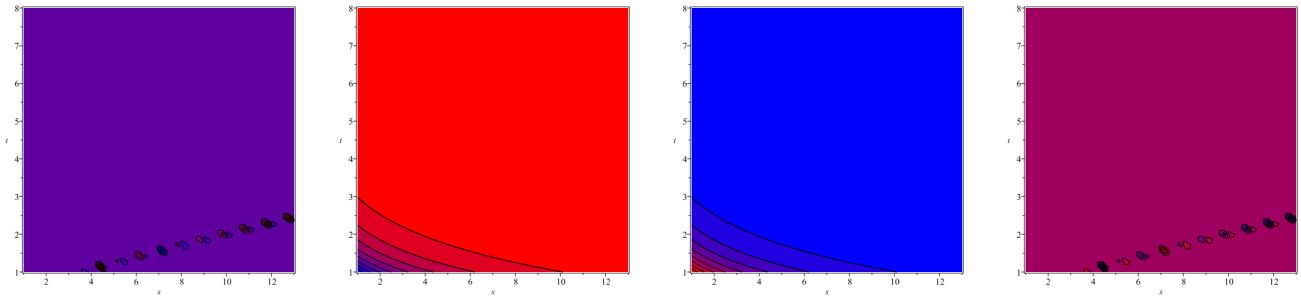

(a) $c = 3$ **(b)** $c = -3$ **(c)** $c = -3$ **(d)** $c = 3$

Figure 4. $\Delta > 0, C_2 = 2C_1, \lambda = \mu = 0.5$ in Tables 2 and 3.

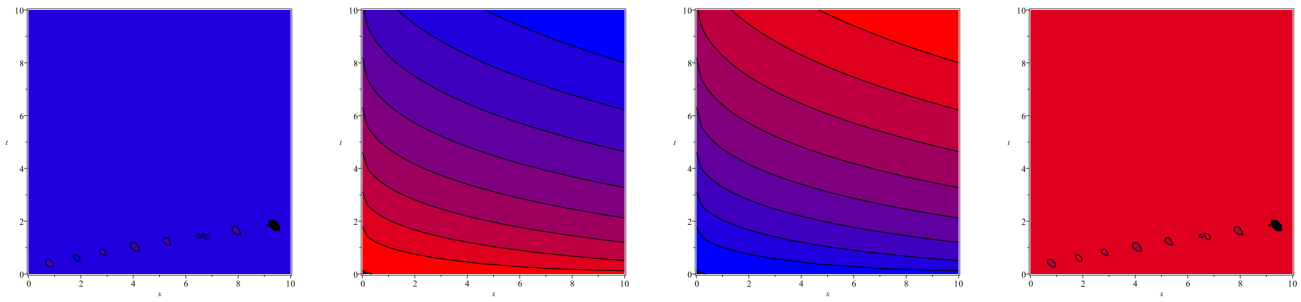

(a) $c = 3$ **(b)** $c = -3$ **(c)** $c = -3$ **(d)** $c = 3$

Figure 5. $\Delta = 0, C_2 = 2C_1, \lambda = \mu = 0.5$ in Tables 2 and 3.

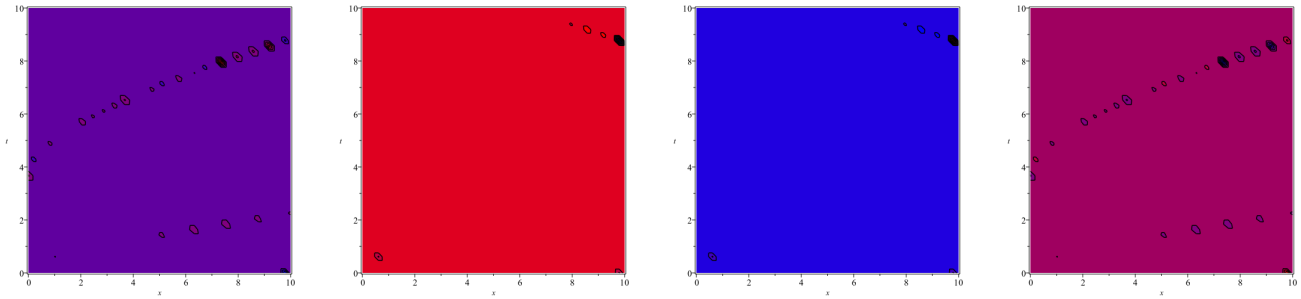

(a) $c = 3$ **(b)** $c = -3$ **(c)** $c = -3$ **(d)** $c = 3$

Figure 6. $\Delta < 0, C_2 = 2C_1, \lambda = \mu = 0.5$ in Tables 2 and 3.

Figure 7–9 show the same scenarios as Figures 1–3, respectively, but with k reduced by a factor of 1000. The corresponding contour plots are shown in Figures 10–12.

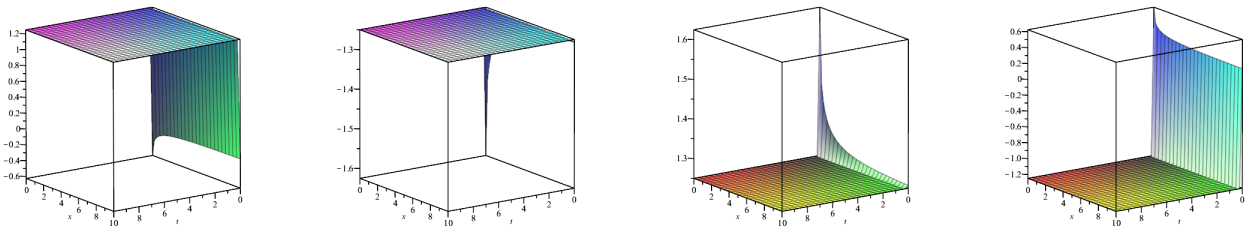

(a) $c = 3000$ **(b)** $c = -3000$ **(c)** $c = -3000$ **(d)** $c = 3000$

Figure 7. $\Delta > 0, C_2 = 2C_1, \lambda = \mu = 0.5$ in Tables 2 and 4.

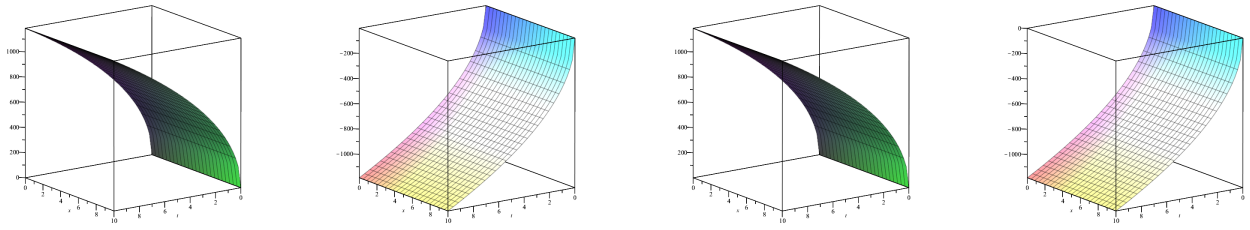

(a) $c = 3000$ **(b)** $c = -3000$ **(c)** $c = -3000$ **(d)** $c = 3000$

Figure 8. $\Delta = 0, C_2 = 2C_1, \lambda = \mu = 0.5$ in Tables 2 and 4.

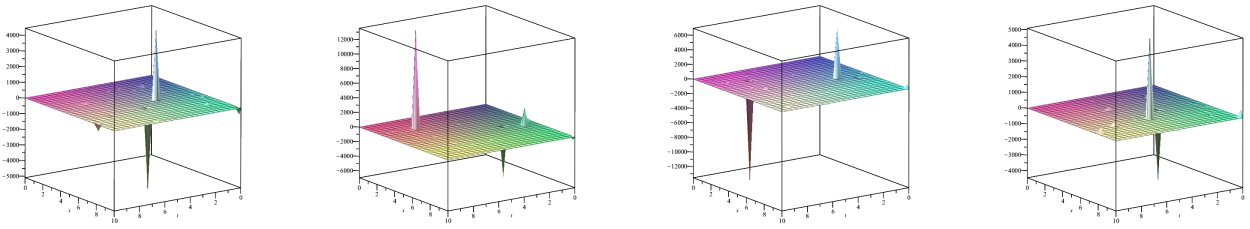

(a) $c = 3000$ **(b)** $c = -3000$ **(c)** $c = -3000$ **(d)** $c = 3000$

Figure 9. $\Delta < 0, C_2 = 2C_1, \lambda = \mu = 0.5$ in Tables 2 and 4.

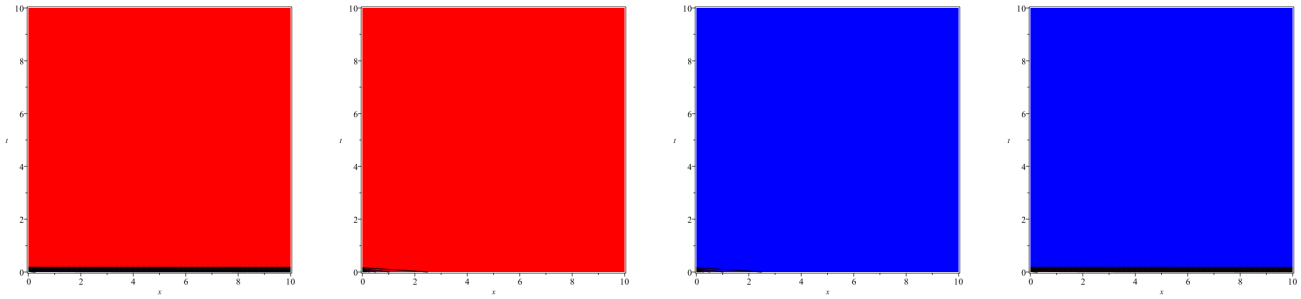

(a) $c = 3000$ **(b)** $c = -3000$ **(c)** $c = -3000$ **(d)** $c = 3000$

Figure 10. $\Delta > 0, C_2 = 2C_1, \lambda = \mu = 0.5$ in Tables 2 and 4.

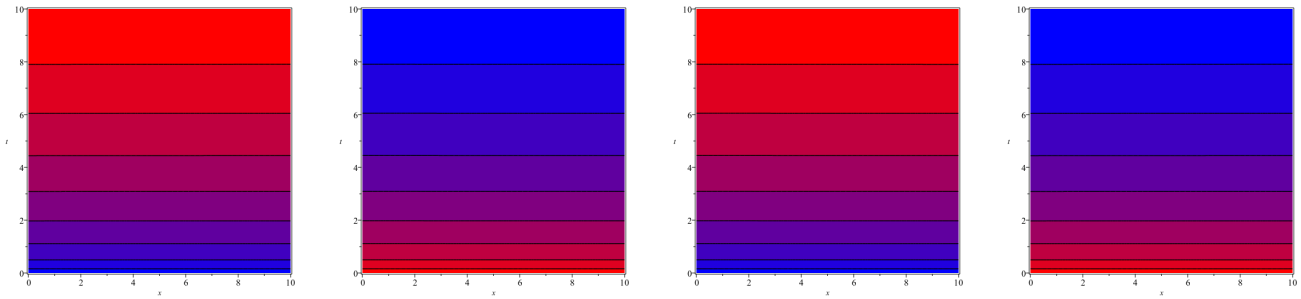

(a) $c = 3000$ **(b)** $c = -3000$ **(c)** $c = -3000$ **(d)** $c = 3000$

Figure 11. $\Delta = 0, C_2 = 2C_1, \lambda = \mu = 0.5$ in Tables 2 and 4.

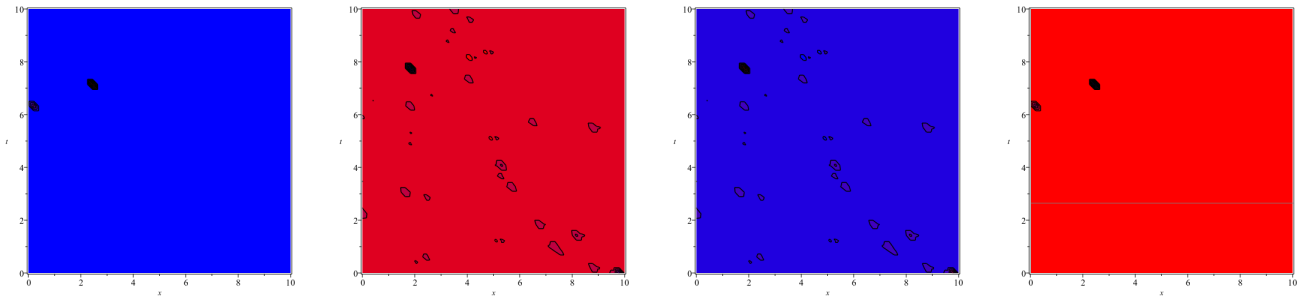

(a) $c = 3000$ **(b)** $c = -3000$ **(c)** $c = -3000$ **(d)** $c = 3000$

Figure 12. $\Delta < 0, C_2 = 2C_1, \lambda = \mu = 0.5$ in Tables 2 and 4.

Figure 13–28 present the three-dimensional surface plots and the corresponding contour plots for the fixed parameters $a = 2, b = 1$, and $k = 1$. Specifically, Figures 13–16 show the results when the fractional orders satisfy $\lambda = \mu$ and increase from 0.1 to 1 in increments of 0.3. Figures 17–28 show the results when λ and μ vary in opposite directions. Together, these figures clearly illustrate how the exact solutions change with the fractional orders, providing an intuitive visualization that helps readers better understand the solution behavior. When $\lambda = \mu = 1$, the corresponding solutions exhibit noticeably poorer regularity. However, when one of the parameters λ or μ is taken as 1 and the other as 0, the regularity region is significantly improved. Furthermore, the comparison shows that the regularity becomes worse as $\frac{\lambda+\mu}{2}$ increases. We also examine the influence of the parameter k on

the solutions: larger values of k introduce more singularities and increase the likelihood of blow-up, whereas smaller values of k mitigate singularities and promote the global existence of solutions. These observations provide valuable insight into the behavior of fractional partial differential equations and offer a theoretical perspective on the underlying physical phenomena.

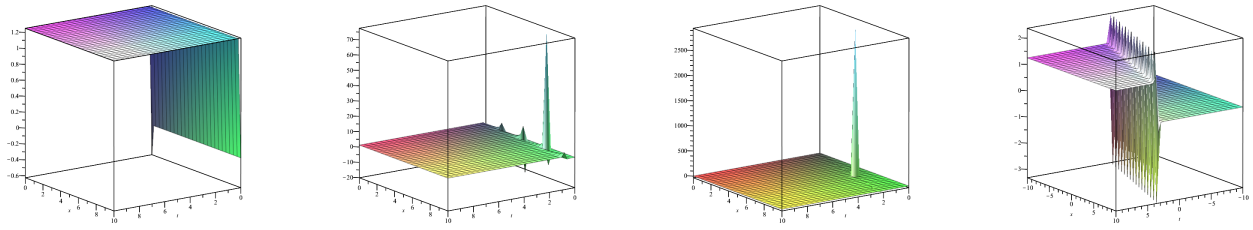

(a) $\lambda = \mu = 0.1$ **(b)** $\lambda = \mu = 0.4$ **(c)** $\lambda = \mu = 0.7$ **(d)** $\lambda = \mu = 1$

Figure 13. $\Delta > 0, c = 3, C_2 = 2C_1$ in Tables 5 and 6.

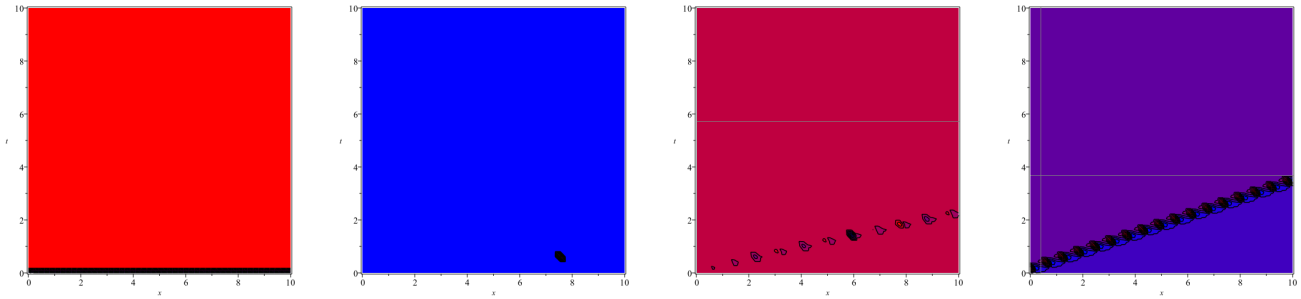

(a) $\lambda = \mu = 0.1$ **(b)** $\lambda = \mu = 0.4$ **(c)** $\lambda = \mu = 0.7$ **(d)** $\lambda = \mu = 1$

Figure 14. $\Delta > 0, c = 3, C_2 = 2C_1$ in Tables 5 and 6.

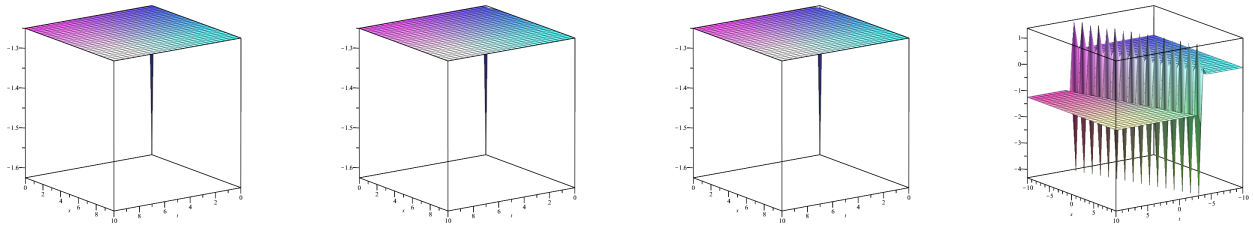

(a) $\lambda = \mu = 0.1$ **(b)** $\lambda = \mu = 0.4$ **(c)** $\lambda = \mu = 0.7$ **(d)** $\lambda = \mu = 1$

Figure 15. $\Delta > 0, c = -3, C_2 = 2C_1$ in Tables 5 and 6.

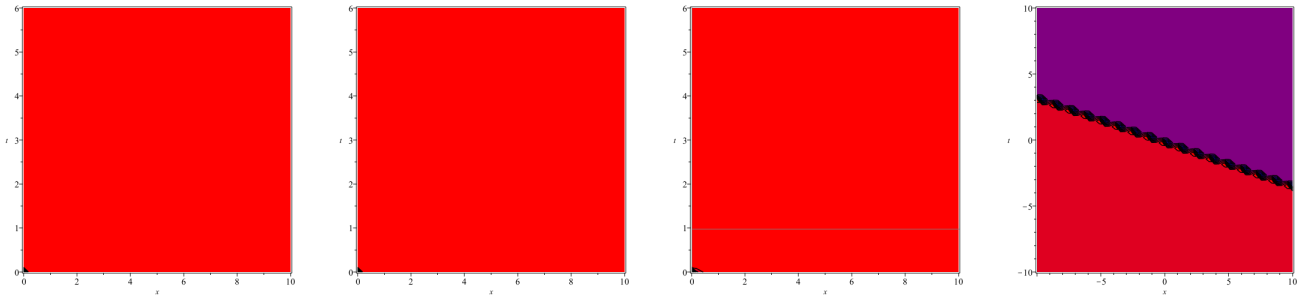

(a) $\lambda = \mu = 0.1$ **(b)** $\lambda = \mu = 0.4$ **(c)** $\lambda = \mu = 0.7$ **(d)** $\lambda = \mu = 1$

Figure 16. $\Delta > 0, c = -3,\ C_2 = 2C_1$ in Tables 5 and 6.

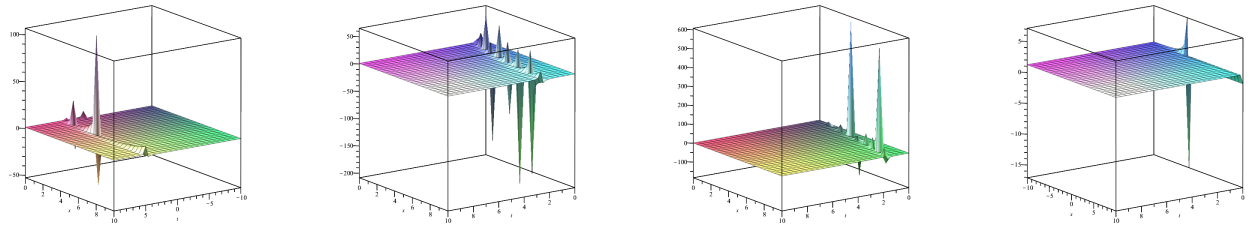

(a) $\lambda = 0.1,\ \mu = 1$ **(b)** $\lambda = 0.4,\ \mu = 0.7$ **(c)** $\lambda = 0.7,\ \mu = 0.4$ **(d)** $\lambda = 1,\ \mu = 0.1$

Figure 17. $\Delta > 0, c = 3, C_2 = 2C_1$ in Tables 5 and 6.

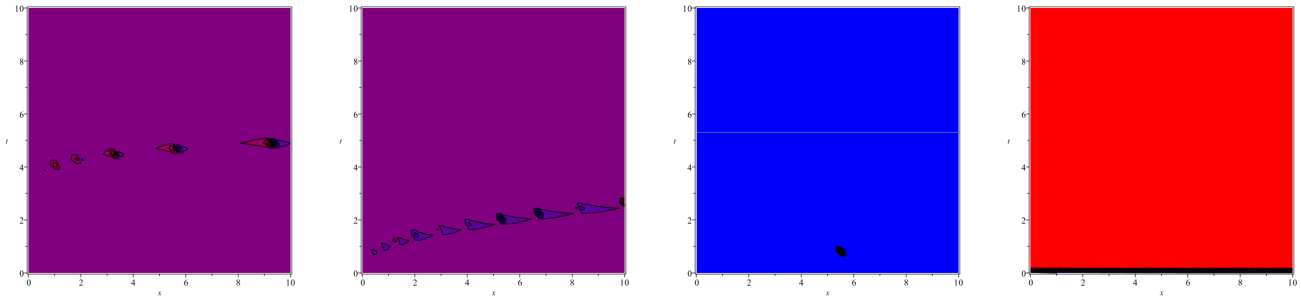

(a) $\lambda = 0.1,\ \mu = 1$ **(b)** $\lambda = 0.4,\ \mu = 0.7$ **(c)** $\lambda = 0.7,\ \mu = 0.4$ **(d)** $\lambda = 1,\ \mu = 0.1$

Figure 18. $\Delta > 0, c = 3, C_2 = 2C_1$ in Tables 5 and 6.

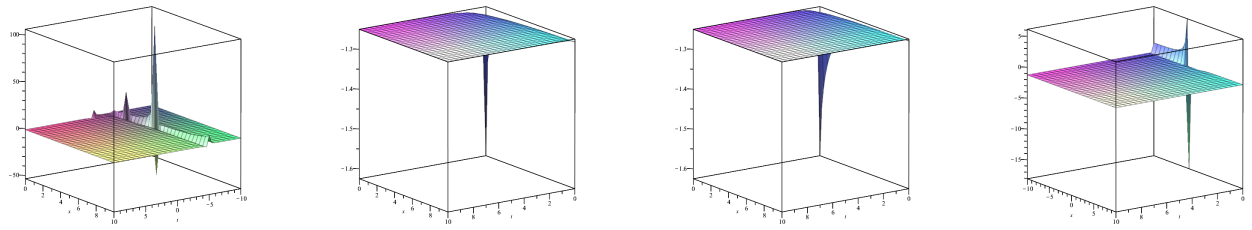

(a) $\lambda = 0.1$, $\mu = 1$ **(b)** $\lambda = 0.4$, $\mu = 0.7$ **(c)** $\lambda = 0.7$, $\mu = 0.4$ **(d)** $\lambda = 1$, $\mu = 0.1$

Figure 19. $\Delta > 0, c = -3, C_2 = 2C_1$ in Tables 5 and 6.

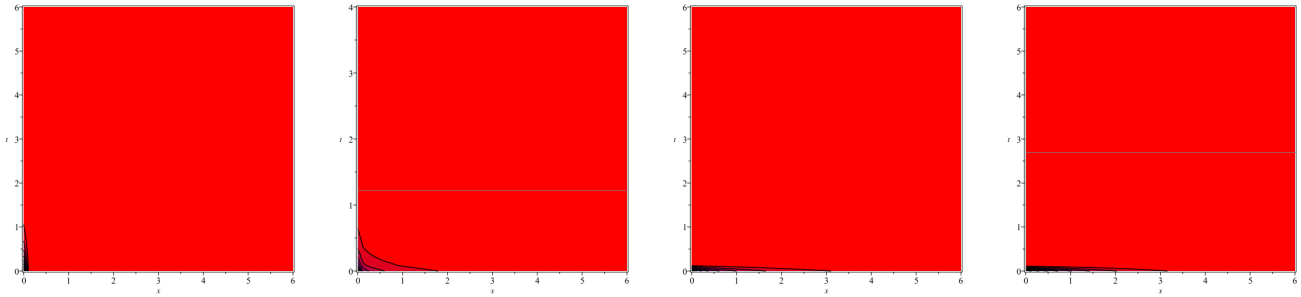

(a) $\lambda = 0.1$, $\mu = 1$ **(b)** $\lambda = 0.4$, $\mu = 0.7$ **(c)** $\lambda = 0.7$, $\mu = 0.4$ **(d)** $\lambda = 1$, $\mu = 0.1$

Figure 20. $\Delta > 0, c = -3, C_2 = 2C_1$ in Tables 5 and 6.

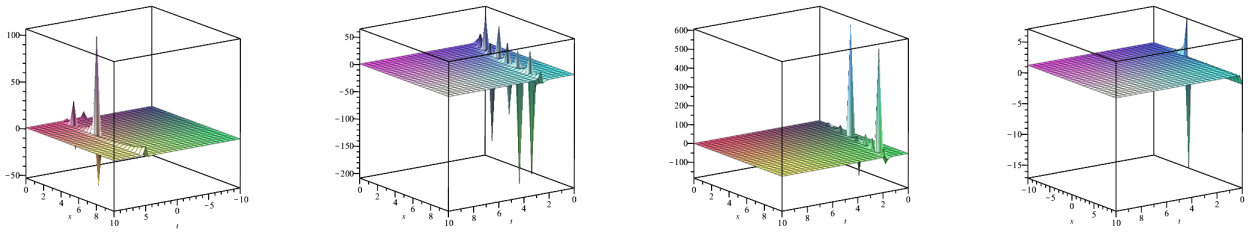

(a) $\lambda = 0.1$, $\mu = 1$ **(b)** $\lambda = 0.4$, $\mu = 0.7$ **(c)** $\lambda = 0.7$, $\mu = 0.4$ **(d)** $\lambda = 1$, $\mu = 0.1$

Figure 21. $\Delta = 0, c = 3, C_2 = 2C_1$ in Tables 5 and 6.

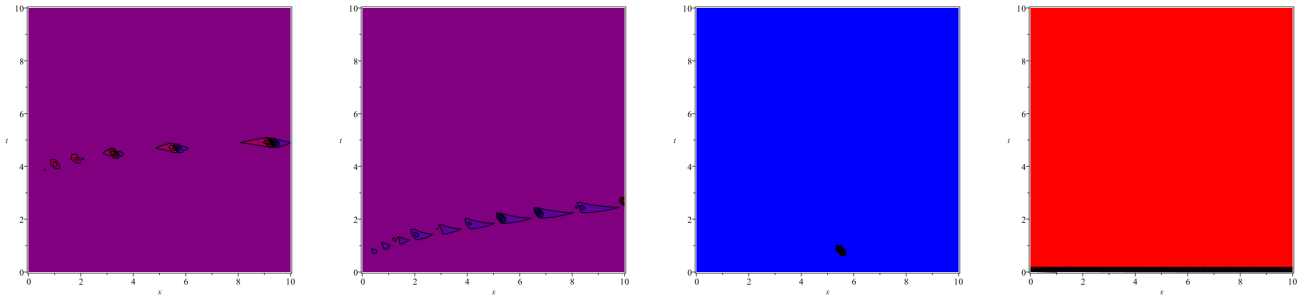

(a) $\lambda = 0.1$, $\mu = 1$ **(b)** $\lambda = 0.4$, $\mu = 0.7$ **(c)** $\lambda = 0.7$, $\mu = 0.4$ **(d)** $\lambda = 1$, $\mu = 0.1$

Figure 22. $\Delta = 0, c = 3, C_2 = 2C_1$ in Tables 5 and 6.

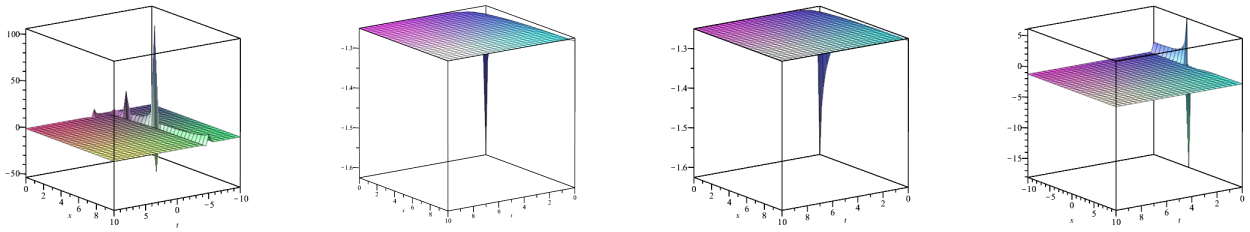

(a) $\lambda = 0.1$, $\mu = 1$ **(b)** $\lambda = 0.4$, $\mu = 0.7$ **(c)** $\lambda = 0.7$, $\mu = 0.4$ **(d)** $\lambda = 1$, $\mu = 0.1$

Figure 23. $\Delta = 0, c = -3, C_2 = 2C_1$ in Tables 5 and 6.

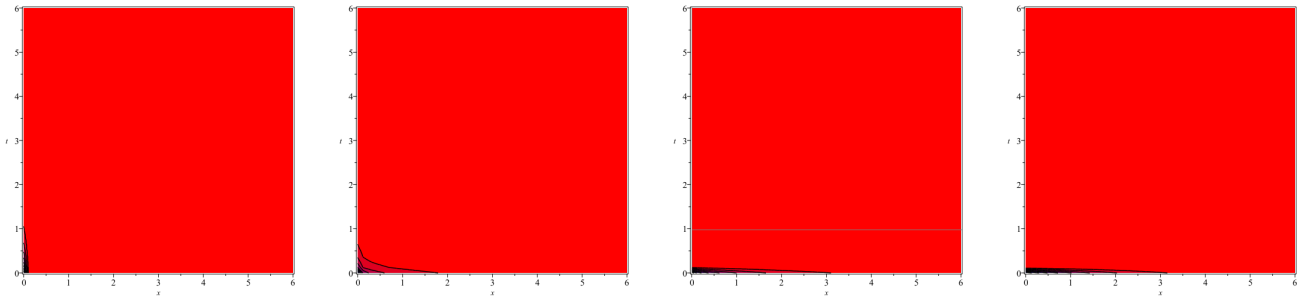

(a) $\lambda = 0.1$, $\mu = 1$ **(b)** $\lambda = 0.4$, $\mu = 0.7$ **(c)** $\lambda = 0.7$, $\mu = 0.4$ **(d)** $\lambda = 1$, $\mu = 0.1$

Figure 24. $\Delta = 0, c = -3, C_2 = 2C_1$ in Tables 5 and 6.

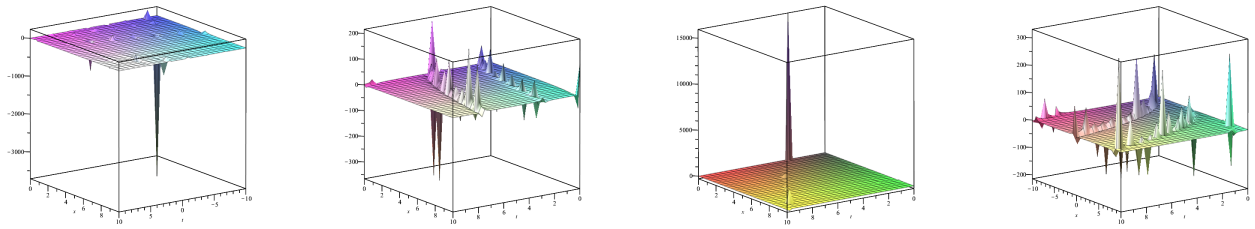

(a) $\lambda = 0.1$, $\mu = 1$ **(b)** $\lambda = 0.4$, $\mu = 0.7$ **(c)** $\lambda = 0.7$, $\mu = 0.4$ **(d)** $\lambda = 1$, $\mu = 0.1$

Figure 25. $\Delta < 0, c = 3, C_2 = 2C_1$ in Tables 5 and 6.

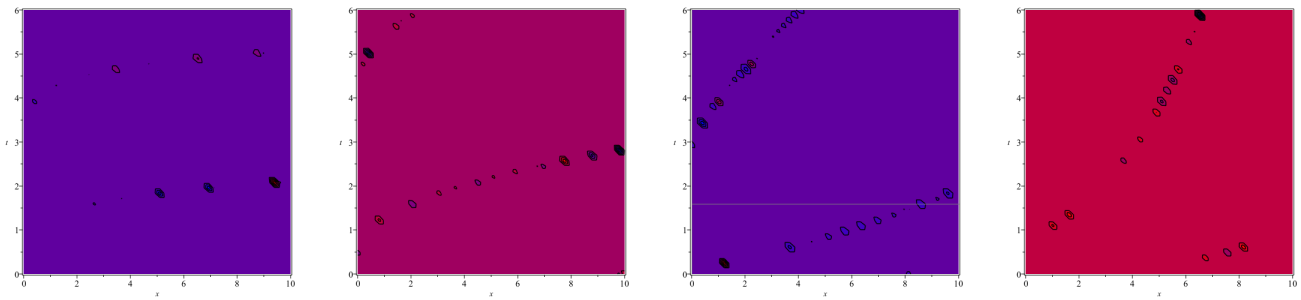

(a) $\lambda = 0.1$, $\mu = 1$ **(b)** $\lambda = 0.4$, $\mu = 0.7$ **(c)** $\lambda = 0.7$, $\mu = 0.4$ **(d)** $\lambda = 1$, $\mu = 0.1$

Figure 26. $\Delta < 0, c = 3, C_2 = 2C_1$ in Tables 5 and 6.

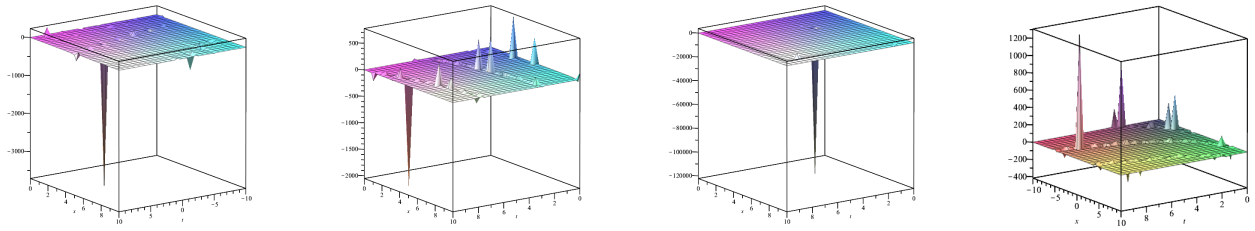

(a) $\lambda = 0.1$, $\mu = 1$ **(b)** $\lambda = 0.4$, $\mu = 0.7$ **(c)** $\lambda = 0.7$, $\mu = 0.4$ **(d)** $\lambda = 1$, $\mu = 0.1$

Figure 27. $\Delta < 0, c = -3, C_2 = 2C_1$ in Tables 5 and 6.

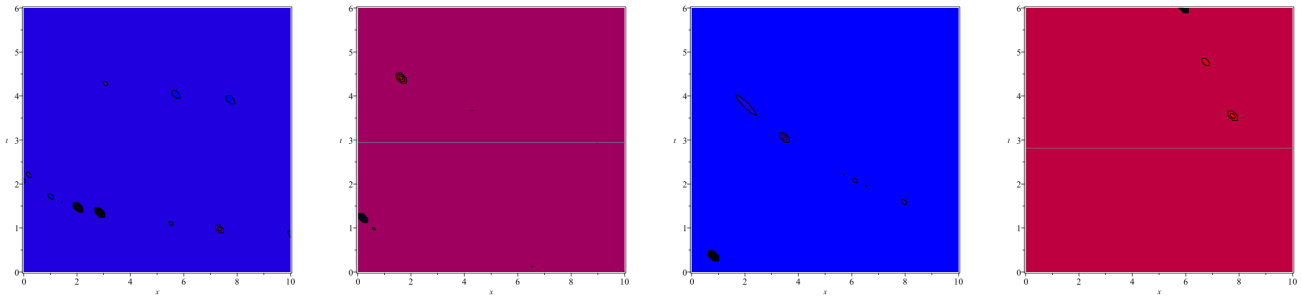

(a) $\lambda = 0.1$, $\mu = 1$ **(b)** $\lambda = 0.4$, $\mu = 0.7$ **(c)** $\lambda = 0.7$, $\mu = 0.4$ **(d)** $\lambda = 1$, $\mu = 0.1$

Figure 28. $\Delta < 0, c = -3, C_2 = 2C_1$ in Tables 5 and 6.

4. Conclusions

The value of the fractional order λ or μ determines the effective contribution, or weight, of the independent variable x or t in forming the traveling-wave coordinate ξ. The closer the order is to 1, the higher the resolution, or magnification factor, of that variable. This mechanism is rooted in the structure of the traveling-wave variable $\xi = \frac{x^\lambda}{\lambda} - c\frac{t^\mu}{\mu}$, where the terms $\frac{x^\lambda}{\lambda}$ and $\frac{t^\mu}{\mu}$ are not simply x and t, but rather distorted coordinates obtained via a power-law transformation. Considering the spatial component $X(x) = \frac{x^\lambda}{\lambda}$, the rate at which this distorted coordinate changes with respect to x is given by its derivative $\frac{dX}{dx} = x^{\lambda-1}$, which serves as the spatial magnification factor. A small fractional order acts as a powerful compressor and smoother. It forces the solution function $u(\xi)$ to vary in a sufficiently gentle and smooth manner within the distorted coordinate system, such that when mapped back to physical space, it exhibits high regularity. In contrast, a large fractional order (close to 1) behaves as a faithful mapper. It does not impose significant compression or smoothing, but instead transmits the true form of $u(\xi)$, which may contain steep gradients almost unchanged to the physical-space solution $u(x, t)$. Consequently, the steep structures inherently generated by the nonlinear equation are fully preserved, leading to poor observed regularity.

As can be seen from the original formulation of the NWSE, the parameter k multiplies the time-derivative term and physically represents the time scale, or relaxation time, of the system. A smaller k implies a smaller coefficient in front of $\partial u/\partial t$, indicating that the system's dynamics evolve faster relative to other processes such as diffusion and reaction. Our finding that decreasing k enhances regularity can therefore be interpreted as follows: when the system's intrinsic dynamics are faster (i.e., smaller relaxation time), the resulting patterns are smoother and more regular. Conversely, when the dynamics are slower (larger k), the system has more time to develop sharp gradients or spikes before being smoothed by diffusion and nonlinear saturation. This interpretation provides a clear physical mechanism underlying the numerical observations and directly links the abstract parameter k to the system's dynamical behavior.

In future work, we aim to extend this analysis to high-dimensional fractional-order equations and also investigate the influence of variations in the parameters a and b on the solution behavior.

Author contributions

Chunyan Zhao: Conceptualization of the methodology and preparation of the original draft. Jie Wu: Formal analysis, and the reviewing, editing, and validation of the manuscript. Zheng Yang: Reviewing and validation of the manuscript.

Use of Generative-AI tools declaration

The authors declare that they have not used Artificial Intelligence (AI) tools in the creation of this article.

Acknowledgments

This work was supported by the National Natural Science Foundation of China (NSFC) through Grants 12271376 (C. Zhao) and 12001384 (Z. Yang).

Conflict of interest

All authors declare no conflicts of interest in this paper.

References

1. M. Abdalla, Z. Liu, H. Hammad, Existence and stability analysis of impusive Caputo fractional delay systems, *Bound. Value Probl.*, **2026** (2026), 32. https://doi.org/10.1186/s13661-025-02214-4
2. I. Ahmad, R. Jan, N. Razak, A. Khab, T. Abdeljawad, Numerical investigation of the dynamical behavior of Hepatitis B virus via Caputo-Fabrizio fractional derivative, *Eur. J. Pure Appl. Math.*, **18** (2025), 5509. https://doi.org/10.29020/nybg.ejpam.v18i1.5509
3. M. Alaroud A comparative analysis using the Laplace transform approach for some nonlinear fractional physical problems, *Part. Differ. Equ. Appl. Math.*, **15** (2025), 101253. https://doi.org/10.1016/j.padiff.2025.101253
4. R. Ali, Z. Zhang, H. Ahmad, M. Alam, The analytical study of soliton dynamics in fractional coupled Higgs system using the generalized Khater method, *OPt. Quant. Electron.*, **56** (2024), 1067. https://doi.org/10.1007/s11082-024-06924-4
5. Y. Alruwaily, R. Alzahrani, F. Alshahrani, B. Meftah, Parametric inequalities for s-convex stochastic processes via Caputo fractional derivatives, *Axioms*, **15** (2026), 147. https://doi.org/10.3390/axioms15020147
6. A. Ambrosetti, P. Rabinowitz, Dual variational methods in critical point theory and applications, *J. Funct. Anal.*, **14** (1973), 349–381. https://doi.org/10.1016/0022-1236(73)90051-7
7. A. Anben, I. Jebril, Z. Dahmani, N. Bedjaoui, A. Lamamri, The Tanh method and the $\frac{G'}{G}$-expansion method for solving the space-time conformable FZK and FZZ evolution equations, *Int. J. Innov. Comput. I.*, **20** (2024), 557–573. https://doi.org/10.24507/ijicic.20.02.557

8. A. Al-Mamun, S. Ananna, P. Protim, T. An, The improved modified extended tanh-function method to develop the exact traveling wave solutions of a family of 3D fractional WBBM equations, *Results Phys.*, **41** (2022), 105969. https://doi.org/10.1016/j.rinp.2022.105969
9. U. Bas, A. Akkurt, A. Has, H. Yildirim, Multiplicative Riemann-Liouville fractional integrals and derivatives, *Chaos Solition. Fract.*, **196** (2025), 116310. https://doi.org/10.1016/j.chaos.2025.116310
10. D. Booth, J. Burkart, X. Cao, et al., A differential harnack inequality for the Newell-Whitehead-Segel equation, *Anal. Theory Appl.*, **35** (2019), 192–204. https://doi.org/10.4208/ata.OA-0005
11. R. Chauhan, Analyzing the memory-based transmission dynamics of Coffee Berry disease using Caputo derivative, *Adv. Theor. Simul.*, **8** (2025), e00373. https://doi.org/10.1002/adts.202500373
12. M. Cortez, M. Yousif, B. Mahmood, P. Mohammed, N. Chorfi, A. Lupas, High-accuracy solutions to the time-fractional Kdv-Burgers equation using rational non-polynominal splines, *Symmetry*, **17** (2025), 16. https://doi.org/10.3390/sym17010016
13. Z. Dahmani, A. Anber, I. Jebril, Solving conformable evolution equations by an extended numerical method, *Jordan J. Math. Stat.*, **15** (2025), 363–380. https://doi.org/10.47013/15.2.14
14. W. Dai, Z. Liu, Classification of nonnegative solutions to static Schrödinger-Hartree and Schrödinger-Maxwell equations with combined nonlinearities, *Calc. Var.*, **58** (2019), 156. https://doi.org/10.1007/s00526-019-1595-z
15. W. Dai, Z. Liu, G. Qin, Classification of nonnegative solutions to static Schrödinger-Hartree-Maxwell type equations, *SIAM J. Math. Anal.*, **53** (2021), 1379–1410. https://doi.org/10.1137/20M1341908
16. H. Durur, Different types analytic solutions of the (1 + 1)-dimensional resonant nonlinear Schrödinger's equation using $\frac{G'}{G}$-expansion method, *Mod. Phys. Lett. B*, **34** (2020), 2050036. https://doi.org/10.1142/S0217984920500360
17. M. Freitag, The fast signal diffusion limit in nonlinear chemotaxis systems, *Discrete Cont. Dyn. B*, **25** (2020), 1109–1128. https://doi.org/10.3934/dcdsb.2019211
18. H. Gandhi, A. Tomar, D. Singh, The comparative study of time fractional linear and nonlinear Newell-Whitehead-Segel equation, In: *Soft computing: Theories and applications*, Singapore: Springer, 2022. https://doi.org/10.1007/978-981-16-1740-9_34
19. Y. Gu, Y. Lai, Analytical investigation of the fractional Klein-Gordon equation along with analysis of bifurcation, sensitivity and chaotic behaviors, *Mod. Phys. Lett. B*, **39** (2025), 2550124. https://doi.org/10.1142/S0217984925501246
20. D. Horstmann, M. Winkler, Boundedness vs. blow-up in a chemotaxis system, *J. Differ. Equations*, **215** (2005), 52–107. https://doi.org/10.1016/j.jde.2004.10.022
21. M. Inc, E. Ulutas, A. Biswas, Singular solitons and other solutions to a couple of nonlinear wave equations, *Chin. Phys. B*, **22** (2013), 060204. https://doi.org/10.1088/1674-1056/22/6/060204
22. Y. Jabri, *The mountain pass theorem: Variants, generalizations and some applications*, Cambridge University Press, 2003.
23. T. Jin, Y. Li, J. Xiong, On a fractional Nirenberg problem, part I: blow up analysis and compactness of solutions, *J. Eur. Math. Soc.*, **16** (2014), 1111–1171. https://doi.org/10.4171/jems/456

24. M. Jornet, J. Nieto, Representation and inequalities involving continuous linear functionals and fractional derivatives, *Adv. Oper. Theory*, **10** (2025), 9. https://doi.org/10.1007/s43036-024-00397-8

25. R. Khalil, M. Al Horani, A. Yousef, M. Sababheh, A new definition of fractional derivative, *J. Comput. Appl. Math.*, **264** (2014), 65–70. https://doi.org/10.1016/j.cam.2014.01.002

26. H. Khan, A. Khan, R. Shah, D. Baleanu, A novel fractional case study of nonlinear dynamics via analytical approach, *Appl. Math. J. Chin. Univ.*, **39** (2024), 276–290. https://doi.org/10.1007/s11766-024-4148-y

27. M. Liaqat, A. Khan, M. Alam, M. K. Pandit, S. Etemad, S. Rezapour, Approximate and closed-form solutions of Newell-Whitehead-Segel equations via modified conformable Shehu transform decomposition method, *Math. Probl. Eng.*, **1** (2022), 6752455. https://doi.org/10.1155/2022/6752455

28. M. Luo, M. Liu, T. Guo, D. Xu, Temporally second-order compact difference method with variable time steps for semi-linear nonlocal Sobolev-type equations, *Commun. Nonlinear Sci.*, **152** (2026), 109155. https://doi.org/10.1016/j.cnsns.2025.109155

29. K. Manikandan, N. Serikbayev, D. Aravinthan, K. Hosseini, Solitary wave solutions of the conformable space-time fractional coupled diffusion equation, *Part. Differ. Equ. Appl. Math.*, **9** (2024), 100630. https://doi.org/10.1016/j.padiff.2024.100630

30. M. Mohammed., Experimental investigation on ultra high-performance concrete beams without shear reinforcement, *Alex. Eng. J.*, **71** (2023), 581–589. https://doi.org/10.1016/j.aej.2023.03.043

31. P. Mohammed, H. Srivastava, D. Baleanu, E. Sarairah, M. Yousif, N. Chorfi, Analytical and approximate monotone solutions of the mixed order fractional nabla operators subject to bounded conditions, *Math. Comp. Model. Dyn.*, **30** (2024), 626–639. https://doi.org/10.1080/13873954.2024.2366335

32. A. Newell, J. Whitehead, Finite bandwidth, finite amplitude convection, *J. Fluid Mech.*, **38** (1969), 279–303. https://doi.org/10.1017/S0022112069000176

33. I. Podlubny, An introduction to fractional derivatives, fractional differential equations, to methods of their solution and some of their applications, *Math. Sci. Eng*, **198** (1999), 340.

34. S. Rametse, R. Herbst, Numerical discretization of Riemann-Liouville fractional derivatives with strictly positive eigenvalues, *Appl. Math.*, **5** (2025), 130. https://doi.org/10.3390/appliedmath5040130

35. R. Ravi, C. Kanchana, P. Siddheshwar, Effects of second diffusing component and cross diffusion on primary and secondary thermoconvective instabilities in couple stress liquids, *Appl. Math. Mech. Engl. Ed.*, **38** (2017), 1579–1600. https://doi.org/10.1007/s10483-017-2280-9

36. R. Santos, J. Sales, G. Santos, Symmetrized neural network operators in fractional calculus: Caputo derivatives, asymptotic analysis, and the Voronovskaya-Santos-Sales theorem, *Axioms*, **14** (2025), 510. https://doi.org/10.3390/axioms14070510

37. I. Sim, S. Tanaka, Positive solutions for fractional-order boundary value problems with or without dependence of integer-order ones, *Fract. Calc. Appl. Anal.*, **29** (2026), 66–100. https://doi.org/10.1007/s13540-026-00483-z

38. S. Tarei, A. Kanaujiya, J. Mohapatra, An efficient numerical solution to generalized New-Whitehead-Segel Equation using Jaiswal-Laguerre functions, *Eng. Computation.*, **42** (2025), 1845–1861. https://doi.org/10.1108/EC-11-2024-1050

39. N. Tuğrul, K. Karacuha, E. Ergün, V. Tabatadze, E. Karacuha, A novel modeling and prediction approach using Caputo derivative: An economical review via multi-deep assessment methodology, *AIMS Math.*, **9** (2024), 23512–23543. https://doi.org/10.3934/math.20241143

40. E. Ünal, A. Gökdoğan, Solution of conformable fractional ordinary differential equations via differential transform method, *Optik*, **128** (2017), 264–273. https://doi.org/10.1016/j.ijleo.2016.10.031

41. K. Wang, S. Li, G. Wang, P. Xu, F. Shi, X. Liu, Localized wave and other special wave solutions to the (3+1)-dimensional Kudryashov-Sinelshchikov equation, *Math. Method. Appl. Sci.*, **48** (2025), 8911–8924. https://doi.org/10.1002/mma.10764

42. K. Wang, X. Liu, F. Shi, G. Li, Bifurcation and sensitivity analysis, chaotic behavior, variational principle, hamiltonian and diverse wave solutions of the new extended integrable Kadomtsev-Petviashvili equation, *Phys. Lett. A*, **534** (2025), 130246. https://doi.org/10.1016/j.physleta.2025.130246

43. K. Wang, An efficient scheme for two different types of fractional evolution equations, *Fractals*, **32** (2024), 2450093. https://doi.org/10.1142/S0218348X24500932

44. K. Wang, New computational approaches to the fractional coupled nonlinear Helmholtz equation, *Eng. Computation.*, **41** (2024), 1285–1300. https://doi.org/10.1108/EC-08-2023-0501

45. M. Wang, X. Li, J. Zhang, The $\frac{G'}{G}$-expansion method and traveling wave solutions of nonlinear evolution equations in mathematical physics, *Phys. Lett. A*, **372** (2008), 417–423. https://doi.org/10.1016/j.physleta.2007.07.051

46. Y. Wang, M. Winkler, Z. Xiang, The fast signal diffusion limit in Keller-Segel(-fluid) systems, *Calc. Var.*, **58** (2019), 196. https://doi.org/10.1007/s00526-019-1656-3

47. M. Wang, Y. Zhou, Z. Li, Application of a homogeneous balance method to exact solutions of nonlinear equations in mathematical physics, *Phys. Lett. A*, **216** (1996), 67–75. https://doi.org/10.1016/0375-9601(96)00283-6

48. M. Winkler, Global large-data solutions in a chemotaxis-(Navier-)Stokes system modeling cellular swimming in fluid drops, *Commun. Part. Diff. Eq.*, **37** (2012), 319–351. https://doi.org/10.1080/03605302.2011.591865

49. J. Wu, Y. Huang, Boundedness of solutions for an attraction-repulsion model with indirect signal production, *Mathematics*, **12** (2024), 1143. https://doi.org/10.3390/math12081143

50. J. Wu, Z. Li, H. Tian, Z. Yang, The extended-$\left(\frac{G'}{G}\right)$-expansion method and new exact solutions for the conformable space-time fractional diffusive predator-prey system, *Sci. Rep.*, **15** (2025), 19053. https://doi.org/10.1038/s41598-025-02856-5

51. J. Wu, Z. Yang, Global existence and boundedness of chemotaxis-fluid equations to the coupled Solow-Swan model, *AIMS Math.*, **8** (2023), 17914–17942. https://doi.org/10.3934/math.2023912

52. W. Wu, L. Zeng, C. Liu, W. Xie, M. Goh, A time power-based grey model with conformable fractional derivative and its applications, *Chaos Soliton. Fract.*, **155** (2022), 111657. https://doi.org/10.1016/j.chaos.2021.111657

53. J. Yin, Extended expansion method for $\frac{G'}{G}$ and new exact solutions of Zakharov equations, *Acta Phys. Sin.*, **62** (2013), 200202. https://doi.org/10.7498/aps.62.200202

54. M. A. Yousif, D. Baleanu, M. Abdelwahed, S. Azzo, P. Mohammed, Finite difference β-fractional approach for solving the time-fractional FitzHugh-Nagumo equation, *Alex. Eng. J.*, **125** (2025), 127–132. https://doi.org/10.1016/j.aej.2025.04.035

55. E. Zayed, K. Gepreel, The $\frac{G'}{G}$-expansion method for finding traveling wave solutions of nonlinear partial differential equations in mathematical physics, *J. Math. Phys.*, **50** (2009), 013502. https://doi.org/10.1063/1.3033750

56. Z. Zhour, N. AI-Mutairi, F. Alrawajeh, R. Alkhasawneh, Series solutions for the Laguerre and Lane-Emden fractional differential equations in the sense of conformable fractional derivative, *Alex. Eng. J.*, **58** (2019), 1413–1420. https://doi.org/10.1016/j.aej.2019.11.012

57. B. Zheng, The $\frac{G'}{G}$-expansion method for solving fractional partial differential equations in the theory of mathematical physics, *Commun. Theor. Phys.*, **58** (2012), 623–630. https://doi.org/10.1088/0253-6102/58/5/02

58. S. Zheng, L. Chen, J. Lu, Numerical analysis of a fractional micro/nano beam-based micro-electromechanical system, *Fractals*, **33** (2025), 2550028. https://doi.org/10.1142/S0218348X25500288

59. S. Zheng, Y. Lou, S. Shen, J. Lu, Numerical investigation of fractal oscillator for a pendulum with a rolling wheel, *Fractals*, **33** (2025), 2550077. https://doi.org/10.1142/S0218348X2550077X

AIMS Press